Check for updates

A defective bismuth–indium catalyst promotes water dissociation for selective carbon dioxide electroreduction to HCOOH†

Jieshu Zhou,[a] Liming Li,[b,c] Hangxing Ren,[b,d] Haibin Wang, [iD][a] Yong Li,[e] Kangning Liu,[a] Liang Huang,[e] Xinyao Yang,[e] Zhen Hao,[b] Yuguang Zhang,[b] Zhichao Wang,[e] Xi Wang,[a] Jian Ding,[e] Yuping Ji,[e] Li Wang[a] and Hongyan Liang [iD] *[a]

Electroreduction of CO_2 to formic acid (HCOOH) is promising for CO_2 utilization but remains a substantial challenge due to the lack of high-efficiency electrocatalysts. Herein, the defective BiIn bimetallic catalyst derived from a P-doped BiIn pre-catalyst is developed, which enables CO_2 conversion to HCOOH with high activity and selectivity. Mechanistic investigations demonstrate that: (i) the interaction between Bi and In orbitals optimizes the adsorption strength of the key intermediate *OCHO; and (ii) the P leakage could induce the generation of defective BiIn during the self-reconstruction process, which strengthens *OH adsorption, resulting in an accelerated water dissociation and promoted CO_2 reduction. The defective BiIn@P catalyst exhibits a 97.3% faradaic efficiency at a current density of 500 mA cm^{-2} in alkaline electrolytes. This work deepens our understanding of the CO_2 reduction mechanism on a BiIn-based catalyst, guiding in the design of advanced CO_2R catalysts.

Introduction

The electrocatalytic carbon dioxide reduction reaction (CO_2RR) provides a clean and sustainable strategy for converting renewable electricity to fuels and chemicals.[1,2] The multi-electron transfer process during the CO_2RR results in multiple possible products simultaneously, including multicarbon (C_{2+}) products (*e.g.*, C_2H_4 and C_2CH_5OH) and monocarbon (C_1) products (*e.g.*, CO and HCOOH).[3,4] Even though compared with the C_1 products, the C_{2+} products exhibit higher commercial value, their faradaic efficiency (FE) is inferior to that of C_1 products (>95%). Formic acid, a main C_1 product of the CO_2RR, is a high-energy-density molecule, which could be used in various industrial applications.[5–8] As a stable liquid product, HCOOH is more favourable for purification, storage and transportation. Thus, techno-economic analysis suggests that the high production rate and good industrial adaptability of

HCOOH make its synthesis economically viable.[9] However, achieving high HCOOH conversion from CO_2 at industrial current densities remains a significant challenge.[10]

Over the past decades, a lot of electrocatalysts have been explored for HCOOH production.[11] P-block metals, such as bismuth (Bi), indium (In), tin (Sn), and lead (Pb), have been widely recognized as efficient catalysts for selective HCOOH generation.[12] Among them, Bi has attracted more attention due to its decent performance, low toxicity and high Earth abundance.[13] However, there is still a lot of room to improve the activity and selectivity of Bi-based catalysts because the weak binding energy of the key intermediate *OCHO limits their catalytic performance.[14,15] Introducing another metallic element with a strong binding energy of *OCHO (*e.g.*, In and Sn) is an effective approach to modify the electronic construction of Bi, resulting in optimized binding energy of *OCHO.[14,15] For example, BiIn binary-component catalysts have been reported to enhance the activity and selectivity for HCOOH production, but achieving high FE over a large current density (>500 mA cm^{-2}) remains a significant challenge.[14]

In addition, water serves as a proton source for the CO_2RR in an alkaline electrolyte; thus the sluggish H_2O dissociation might hinder the total reaction rate.[16–18] Recent reports have demonstrated that improving *OH adsorption could accelerate water dissociation, which is beneficial for HCOOH formation.[19,20] Moreover, the metal defects on Bi-based catalyst surfaces caused enhanced adsorption of *OH, resulting in

[a]School of Materials Science and Engineering, Tianjin University, Tianjin 300350, P. R. China. E-mail: hongyan.liang-tju@edu.cn
[b]PERIC Hydrogen Technologies Co., Ltd, Handan 056000, P. R. China
[c]School of Chemical Engineering and Technology, Tianjin University, Tianjin 300072, P.R. China
[d]School of Materials Science and Engineering, Shanghai Jiao Tong University, Shanghai 200240, P.R. China
[e]CETC Deqing Huaying Electronics Co., Ltd, Deqing, Zhejiang, 313200, P.R.China
†Electronic supplementary information (ESI) available. See DOI: https://doi.org/10.1039/d4qi00053f

This journal is © the Partner Organisations 2024

Inorg. Chem. Front., 2024, **11**, 1703–1709 | **1703**

promoted CO_2RR to $HCOOH$.[10] Utilization of metallic defects to strengthen the *OH adsorption and accelerate H_2O dissociation could be an efficient strategy for boosted CO_2RR to HCOOH, but it has not been investigated sufficiently. From this perspective, constructing defective catalysts for promoted water dissociation and HCOOH production, and understanding the mechanism are highly desirable.

Herein, starting from BiIn catalysts, we investigated the effect of defective surfaces on promoting HCOOH production. Phosphorus (P) was doped in a BiIn pre-catalyst as a sacrificial reagent for constructing a defective surface. During the spontaneous self-reconstruction in the catalyst activation process, P leaks into the electrolyte, leading to a defective BiIn structure. *In situ* Raman spectroscopy combined with isotopic labelling experiments demonstrated that the defective sites can strengthen *OH adsorption and promote H_2O dissociation, thereby accelerating the kinetics of the CO_2RR. Density functional theory (DFT) calculations revealed the crucial role of defective BiIn dual-metal sites in water dissociation and CO_2RR kinetics, which agreed with the experimental conclusions. As a result, the optimized catalyst achieves a FE_{HCOOH} of 97.3% at a current density of 500 mA cm^{-2} with a production rate of 9483 μmol h^{-1} cm^{-2}.

Results and discussion

Preparation and characterization of BiIn-P pre-catalysts

To obtain defective BiIn@P catalysts, BiIn-P pre-catalysts were synthesized firstly *via* a solvothermal reduction (Fig. 1a and Fig. S1†). For comparison, Bi–P, In–P and BiIn pre-catalysts

were synthesized as control samples (Fig. S2†). The X-ray diffraction (XRD) patterns in Fig. 1b and S3† reveal that the BiIn-P pre-catalyst is poorly crystalline. However, significant diffraction peaks corresponding to the metallic Bi (PDF# 44-1246) were observed in the XRD patterns of BiIn and Bi–P control pre-catalysts. X-ray photoelectron spectroscopy (XPS) characterization was carried out for elemental composition analysis. The survey spectrum in Fig. S4† demonstrates the co-existence of Bi, In and P elements in the BiIn-P pre-catalyst. The high-resolution XPS of Bi 4f (164.4/159.2 eV), In 3d (452.5/445.1 eV), and P 2p (134.8/133.9 eV) in Fig. 1c–e further indicated that Bi, In, and P species are the components of the BiIn-P pre-catalyst.[21–23]

CO_2 electroreduction performance

The CO_2RR performance of BiIn-P and the control samples were evaluated in a 1.0 M KOH electrolyte with a flow-cell system (Fig. 2a). BiIn-P showed the highest current density under the same potential compared to control samples in linear sweep voltammetry (LSV) curves (Fig. S5†). For all catalysts, only H_2 and CO were observed in the gaseous product, while $HCOO^-$ is the only detected liquid product (Fig. S6 and S7†). The amount of other products is too low to be detected under our experimental conditions. Furthermore, BiIn-P exhibited over 95% FE_{HCOOH} in a wide range of current densities, which reached up to 97.3% at a current density of 500 mA cm^{-2} (Fig. 2b). Moreover, BiIn-P achieved a partial current density of HCOOH up to 486 mA cm^{-2} at a potential of −0.92 V *vs.* reversible hydrogen electrode (RHE, unless otherwise specified), which is higher than that of control samples (Fig. 2c). Therefore, the production rate of HCOOH over BiIn-P
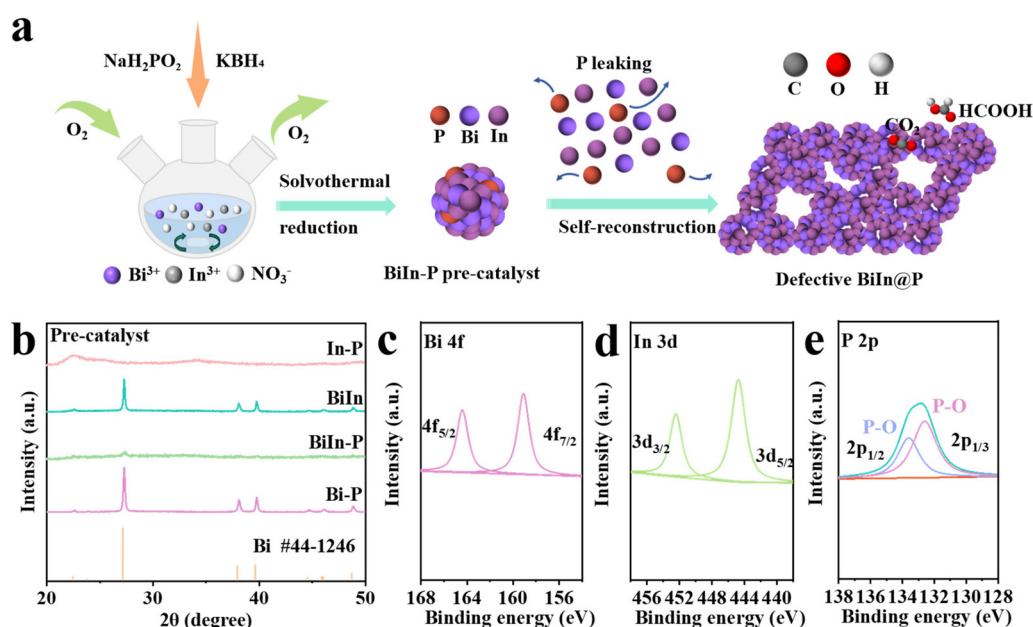
Fig. 1 (a) Illustration of the synthetic process and electrochemical reconstruction of the BiIn-P pre-catalyst. (b) XRD patterns of various pre-catalysts. High-resolution XPS spectra of (c) Bi 4f, (d) In 3d, and (e) P 2p in the BiIn-P pre-catalyst.
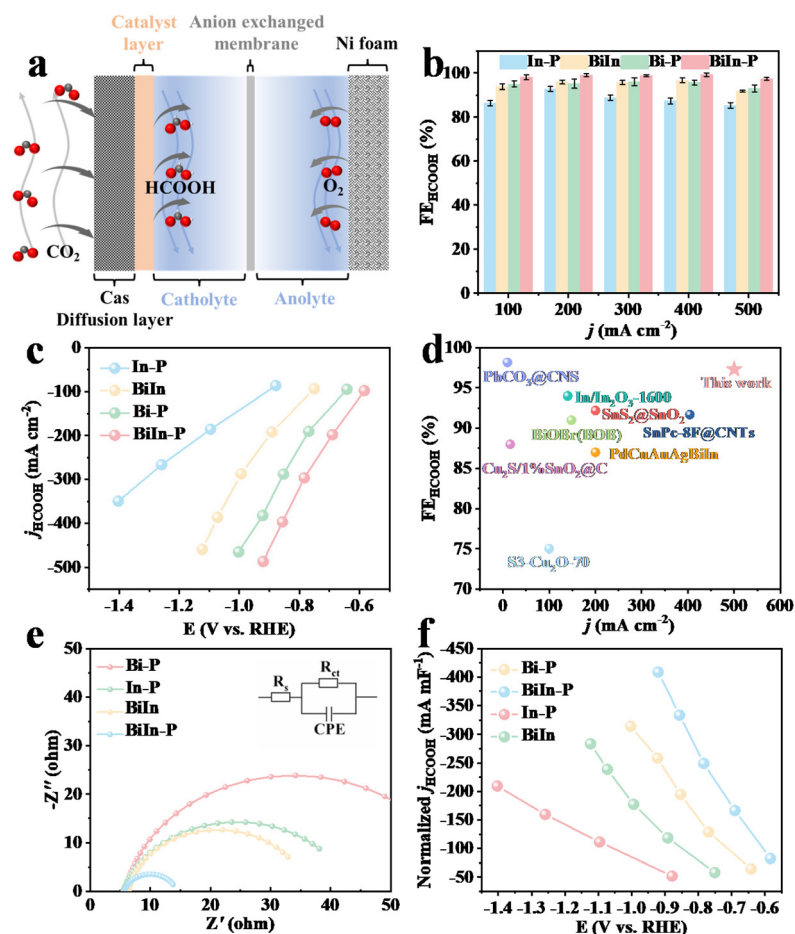
Fig. 2 (a) Schematic diagram of CO_2 reduction in a flow-cell. (b) Comparison of the FE_{HCOOH} of In−P, BiIn, Bi−P, and BiIn-P at various current densities. (c) Partial current densities of HCOOH for In−P, BiIn, Bi−P, and BiIn-P at different potentials. (d) Comparison of the performance with those of other reported catalysts. (e) Nyquist plots of the catalysts in 1.0 M KOH at −0.8 V vs. Ag/AgCl. (f) Partial current densities of HCOOH for catalysts normalized by the C_{dl}.

can reach 9483 μmol h⁻¹ cm⁻² at −0.92 V (Fig. S8†). BiIn-P outperformed the reported catalysts in terms of the current density and FE_{HCOOH} (Fig. 2d and Table S1†).

We then evaluated the stability of BiIn-P in a membrane electrode assembly (MEA) electrolyser using 0.1 M $KHCO_3$ as the electrolyte (Fig. S9†). BiIn-P exhibited an initial FE_{HCOOH} exceeding 92% and the FE_{HCOOH} remained over 80% for 17 hours (Fig. S10†). Fig. 2e shows that the Nyquist plot of BiIn-P displays the smallest diameter of the semicircle, indicating the lowest R_{ct} value, which is favorable for charge transfer during CO_2 electroreduction.[24] To better evaluate the intrinsic selectivity and activity of BiIn-P, we measured the electrochemically active surface area (ECSA) using the double-layer capacitance (C_{dl}). The value of C_{dl} was determined through cyclic voltammetry (CV) at different rates (Fig. S11†). To eliminate the possibility that the improved activity may be ascribed to the increase of the catalyst's surface area, we normalized the partial current density of HCOOH by the ESCA. BiIn-P showed the highest partial current density compared to control samples under the same potential (Fig. 2f). Therefore, BiIn-P

exhibited better intrinsic CO_2 electroreduction activity than the control samples.

Characterization of the catalyst after the reaction and mechanistic understanding

To investigate the BiIn-P pre-catalyst's evolution and gain mechanistic understanding, we conducted a series of in situ electrochemical spectroscopy studies and subsequent CO_2RR characterization of BiIn-P. The XRD pattern of BiIn-P after the CO_2RR demonstrated the existence of the Bi_3In_5 phase, with two typical peaks located at 31.5° and 33.1°, which are indexed to the (213) and (310) planes (Fig. 3a). Meanwhile, the XRD peaks of Bi−P, In−P, and BiIn after the reaction are indexed to Bi, In, Bi_3In_5 and BiIn, respectively (Fig. S12†). The transmission electron microscopy (TEM) image and energy dispersive spectrum (EDS) demonstrated the uniform distribution of Bi and In elements with an atomic ratio of ~1 : 1.49 (Fig. S13†). To further investigate the effects of introducing P on the structural reconstruction of BiIn-P pre-catalysts, we conducted XPS and electron spin resonance (EPR) measurements.
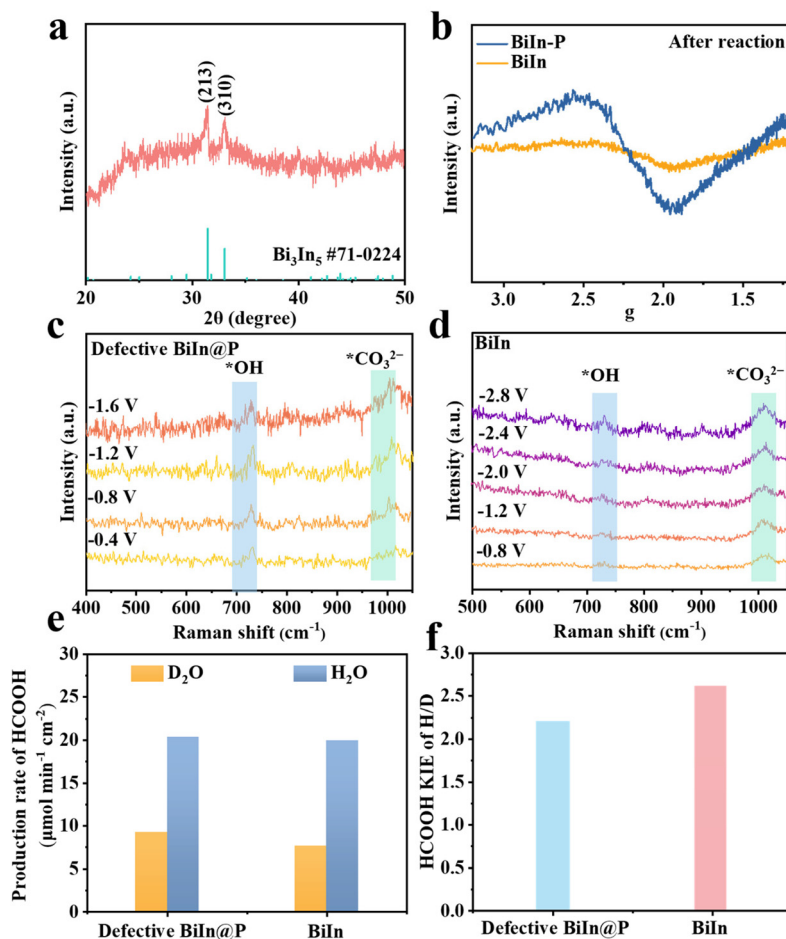
Fig. 3 (a) XRD pattern of BiIn-P after the reaction. (b) EPR spectra of BiIn-P and BiIn after the reaction. *In situ* Raman spectra of (c) defective BiIn@P and (d) BiIn collected in a CO_2-flowed 0.1 M $KHCO_3$ electrolyte at different potentials *vs.* RHE. (e) The production rates of HCOOH in H_2O and D_2O at −0.88 V. (f) The KIE values of different catalysts.

A strong peak located at ~2.2 (g value) appeared (Fig. 3b), indicating the generation of a large number of metal defects during the reaction.[25] Moreover, the signal of P in XPS disappeared (Fig. S14†), revealing that P leaked from the BiIn-P pre-catalyst under the reduction potential, which is expected to be the reason for the generation of defective BiIn@P catalysts.

We then tracked the *OH adsorption using electrochemical spectroscopy techniques. The *in situ* Raman spectra in Fig. 3c and d show the signals of *OH and $*CO_3^{2-}$ at ~730 and ~1006 cm^{-1}, respectively.[26,27] It is noted that, compared with the BiIn pre-catalyst derived sample, the Raman peak of *OH on the BiIn-P derived sample appeared at a lower potential with a higher intensity, indicating that the defective surface can promote *OH adsorption. *OH adsorption over defective BiIn@P and BiIn was further investigated through conducting LSV in Ar-saturated 1.0 M KOH solutions.[28] As can be seen from Fig. S15,† defective BiIn@P exhibits a stronger peak compared to BiIn, which implies that the introduction of defects strengthens the *OH adsorption.[20] Subsequently, kinetic isotopic effect (KIE) experiments were conducted by comparing the reaction rates in electrolytes with H_2O and D_2O to study the

effects of water dissociation and proton transfer in the CO_2RR (Fig. 3e and f).[20] A higher KIE value reveals a stronger impact of water dissociation on the CO_2RR.[29] The KIE value of BiIn was 2.62, suggesting that the reaction rate of the CO_2RR is limited by water dissociation (Fig. 3f). With the introduction of defects, the KIE value of defective BiIn@P decreased to 2.20, indicating that the generation of defects can promote water dissociation and subsequently enhance the CO_2RR rate (Fig. 3f).[20,29]

DFT calculations

To further understand the fundamental mechanism of the high HCOOH selectivity on defective BiIn@P catalysts, the effects of BiIn dual-metal sites and defects on the catalysts were investigated by DFT. As shown in Fig. 4a, the Bi–Bi dual-metal site exhibits weak adsorption of *OCHO, while the In–In dual-metal site shows strong adsorption of *OCHO. The Bi–In dual-metal site exhibits moderate adsorption of *OCHO, which is favourable for HCOOH generation (Fig. 4a and Fig. S16†).
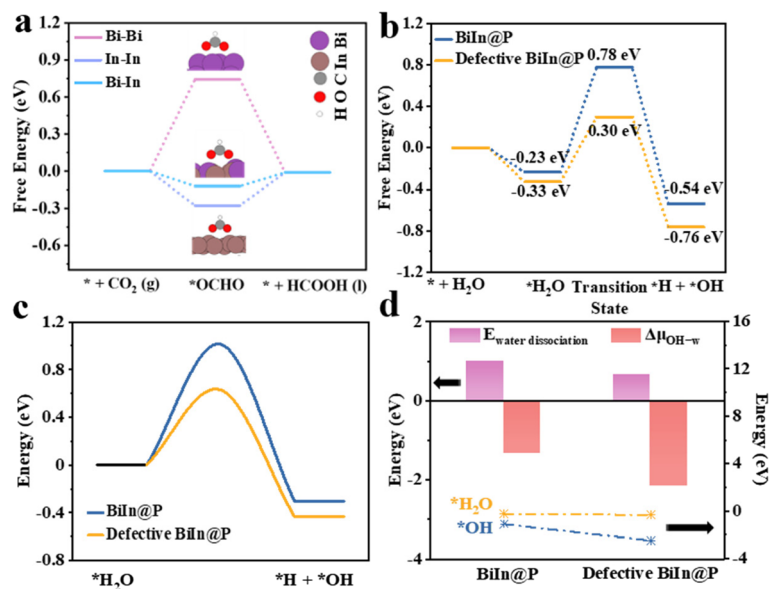
Fig. 4 (a) Formation energy of HCOOH on Bi, In, and Bi_3In_5 surfaces without applying any external potential ($U = 0$ eV). (b) Reaction energy for H_2O adsorption and dissociation on BiIn@P and defective BiIn@P surfaces. (c) The transition barrier investigation for H_2O dissociation on BiIn@P and defective BiIn@P. (d) The reaction energy for H_2O dissociation and free energy of $\Delta\mu_{OH-w}$, the adsorption energy of *OH and the adsorption energy of *H_2O for BiIn@P and defective BiIn@P.

Subsequently, we investigate the effects of defects on H_2O dissociation (Fig. S17†), which is crucial for the overall reaction rates of the CO_2RR. Fig. 4b and c illustrate that the energy barrier for H_2O dissociation on the defective BiIn@P surface is 0.66 eV, which is smaller than that on the BiIn@P surface (1.01 eV). In order to figure out the relationship between defects and promote the water dissociation effect, the chemical potential difference between *H_2O and *OH (denoted as $\Delta\mu_{OH-w}$) was obtained (Fig. 4d). This indicator has recently been used to reflect the water dissociation ability.[20] Fig. 4d shows that the adsorption energy of *OH significantly decreases on the defective sites, while the change in the adsorption energy of water is limited. Thereby, the reduced $\Delta\mu_{OH-w}$ predominantly originates from the strengthened *OH adsorption, which leads to the decrease of $\Delta\mu_{OH-w}$ and easier CO_2 protonation.

density of 500 mA cm^{-2}. This work highlights the importance of water dissociation during the CO_2RR, and opens a new strategy for designing advanced CO_2R catalysts.

Author contributions

Jieshu Zhou performed DFT calculations and carried out the electrochemical experiments. Liming Li, Hangxing Ren, Yong Li, Liang Huang, Xinyao Yang, Zhen Hao, Yuguang Zhang, Zhichao Wang, Jian Ding, and Yuping Ji conducted the characterization. Haibin Wang contributed to electrochemical data analysis and manuscript editing. Kangning Liu and Xi Wang contributed to manuscript editing. Li Wang contributed to electrochemical data collection. Hongyan Liang guided the whole project and revised the paper.

Conclusions

In summary, we developed a P-doped BiIn pre-catalyst derived defective BiIn bimetallic catalyst for HCOOH generation. *In situ* Raman combined with isotopic labelling shows that the introduction of high-defect sites can promote *OH adsorption and H_2O dissociation, thereby accelerating the kinetics of the CO_2RR. DFT calculations revealed the crucial role of BiIn dual-metal sites and defects in promoting CO_2RR kinetics: the Bi–In interaction optimized the *OCHO adsorption, while the introduction of defects expedited the water dissociation kinetics through strengthened *OH adsorption. As a result, the optimized catalyst achieves a FE_{HCOOH} of 97.3% at a current

Conflicts of interest

The authors declare that they have no known competing financial interests or personal relationships that could have appeared to influence the work reported in this paper.

Acknowledgements

This journal is © the Partner Organisations 2024

Inorg. Chem. Front., 2024, **11**, 1703–1709 | **1707**

References

1 P.-P. Yang and M.-R. Gao, Enrichment of reactants and intermediates for electrocatalytic CO_2 reduction, *Chem. Soc. Rev.*, 2023, **52**, 4343–4380.

2 K. Yao, J. Li, H. Wang, R. Lu, X. Yang, M. Luo, N. Wang, Z. Wang, C. Liu, T. Jing, S. Chen, E. Cortés, S. A. Maier, S. Zhang, T. Li, Y. Yu, Y. Liu, X. Kang and H. Liang, Mechanistic Insights into OC–COH Coupling in CO_2 Electroreduction on Fragmented Copper, *J. Am. Chem. Soc.*, 2022, **144**, 14005–14011.

3 N. Han, M. Sun, Y. Zhou, J. Xu, C. Cheng, R. Zhou, L. Zhang, J. Luo, B. Huang and Y. Li, Alloyed Palladium–Silver Nanowires Enabling Ultrastable Carbon Dioxide Reduction to Formate, *Adv. Mater.*, 2021, **33**, 2005821.

4 S. Dey, F. Masero, E. Brack, M. Fontecave and V. Mougel, Electrocatalytic metal hydride generation using CPET mediators, *Nature*, 2022, **607**, 499–506.

5 E. Huttunen-Saarivirta, V. T. Kuokkala, J. Kokkonen and H. Paajanen, Corrosion effects of runway de-icing chemicals on aircraft alloys and coatings, *Mater. Chem. Phys.*, 2011, **126**, 138–151.

6 J. H. Koh, D. H. Won, T. Eom, N.-K. Kim, K. D. Jung, H. Kim, Y. J. Hwang and B. K. Min, Facile CO_2 Electro-Reduction to Formate via Oxygen Bidentate Intermediate Stabilized by High-Index Planes of Bi Dendrite Catalyst, *ACS Catal.*, 2017, **7**, 5071–5077.

7 M. Wesselmark, C. Lagergren and G. Lindbergh, Methanol and formic acid oxidation in zinc electrowinning under process conditions, *J. Appl. Electrochem.*, 2008, **38**, 17–24.

8 Z. Cheng, Q. Dong, G. Pu, J. Song, W. Zhong and J. Wang, A Durable and High-Voltage Mn–Graphite Dual-Ion Battery Using Mn-Based Hybrid Electrolytes, *Small*, 2024, 2400389.

9 O. S. Bushuyev, P. De Luna, C. T. Dinh, L. Tao, G. Saur, J. van de Lagemaat, S. O. Kelley and E. H. Sargent, What Should We Make with CO_2 and How Can We Make It?, *Joule*, 2018, **2**, 825–832.

10 J. Zhu, J. Li, R. Lu, R. Yu, S. Zhao, C. Li, L. Lv, L. Xia, X. Chen, W. Cai, J. Meng, W. Zhang, X. Pan, X. Hong, Y. Dai, Y. Mao, J. Li, L. Zhou, G. He, Q. Pang, Y. Zhao, C. Xia, Z. Wang, L. Dai and L. Mai, Surface passivation for highly active, selective, stable, and scalable CO_2 electroreduction, *Nat. Commun.*, 2023, **14**, 4670.

11 J. Gao, S. Choo Sze Shiong and Y. Liu, Reduction of CO_2 to chemicals and Fuels: Thermocatalysis versus electrocatalysis, *Chem. Eng. J.*, 2023, **472**, 145033.

12 P. Li, F. Yang, J. Li, Q. Zhu, J. W. Xu, X. J. Loh, K.-W. Huang, W. Hu and J. Lu, Nanoscale Engineering of P-Block Metal-Based Catalysts Toward Industrial-Scale Electrochemical Reduction of CO_2, *Adv. Energy Mater.*, 2023, **13**, 2301597.

13 S. Yang, H. An, S. Arnouts, H. Wang, X. Yu, J. de Ruiter, S. Bals, T. Altantzis, B. M. Weckhuysen and W. van der Stam, Halide-guided active site exposure in bismuth electrocatalysts for selective CO_2 conversion into formic acid, *Nat. Catal.*, 2023, **6**, 796–806.

14 K. Yao, H. Wang, X. Yang, Y. Huang, C. Kou, T. Jing, S. Chen, Z. Wang, Y. Liu and H. Liang, Metal-organic framework derived dual-metal sites for electroreduction of carbon dioxide to HCOOH, *Appl. Catal., B*, 2022, **311**, 121377.

15 L. Li, A. Ozden, S. Guo, F. P. García de Arquer, C. Wang, M. Zhang, J. Zhang, H. Jiang, W. Wang, H. Dong, D. Sinton, E. H. Sargent and M. Zhong, Stable, active CO_2 reduction to formate via redox-modulated stabilization of active sites, *Nat. Commun.*, 2021, **12**, 5223.

16 J. Zhang, T. Fan, P. Huang, X. Lian, Y. Guo, Z. Chen and X. Yi, Electro-Reconstruction-Induced Strain Regulation and Synergism of Ag-In-S toward Highly Efficient CO_2 Electrolysis to Formate, *Adv. Funct. Mater.*, 2022, **32**, 2113075.

17 D. M. Koshy, S. A. Akhade, A. Shugar, K. Abiose, J. Shi, S. Liang, J. S. Oakdale, S. E. Weitzner, J. B. Varley, E. B. Duoss, S. E. Baker, C. Hahn, Z. Bao and T. F. Jaramillo, Chemical Modifications of Ag Catalyst Surfaces with Imidazolium Ionomers Modulate H_2 Evolution Rates during Electrochemical CO_2 Reduction, *J. Am. Chem. Soc.*, 2021, **143**, 14712–14725.

18 X. Wang, Y. Wang, X. Sang, W. Zheng, S. Zhang, L. Shuai, B. Yang, Z. Li, J. Chen, L. Lei, N. M. Adli, M. K. H. Leung, M. Qiu, G. Wu and Y. Hou, Dynamic Activation of Adsorbed Intermediates via Axial Traction for the Promoted Electrochemical CO_2 Reduction, *Angew. Chem., Int. Ed.*, 2021, **60**, 4192–4198.

19 W. Ma, S. Xie, X.-G. Zhang, F. Sun, J. Kang, Z. Jiang, Q. Zhang, D.-Y. Wu and Y. Wang, Promoting electrocatalytic CO_2 reduction to formate via sulfur-boosting water activation on indium surfaces, *Nat. Commun.*, 2019, **10**, 892.

20 X. Chen, J. Chen, H. Chen, Q. Zhang, J. Li, J. Cui, Y. Sun, D. Wang, J. Ye and L. Liu, Promoting water dissociation for efficient solar driven CO_2 electroreduction via improving hydroxyl adsorption, *Nat. Commun.*, 2023, **14**, 751.

21 C. Kou, J. Zhou, H. Wang, J. Han, M. Han, A. Vomiero, Y. Liu and H. Liang, Boron pretreatment promotes phosphorization of FeNi catalysts for oxygen evolution, *Appl. Catal., B*, 2023, **330**, 122598.

22 J. E. Pander III, M. F. Baruch and A. B. Bocarsly, Probing the Mechanism of Aqueous CO_2 Reduction on Post-Transition-Metal Electrodes using ATR-IR Spectroelectrochemistry, *ACS Catal.*, 2016, **6**, 7824–7833.

23 D. Tan, W. Lee, Y. E. Kim, Y. N. Ko, M. H. Youn, Y. E. Jeon, J. Hong, J. E. Park, J. Seo, S. K. Jeong, Y. Choi, H. Choi, H. Y. Kim and K. T. Park, In–Bi Electrocatalyst for the Reduction of CO_2 to Formate in a Wide Potential Window, *ACS Appl. Mater. Interfaces*, 2022, **14**, 28890–28899.

24 Y. Feng, N. Ran, X. Wang, Q. Liu, J. Wang, L. Liu, K. Suenaga, W. Zhong, R. Ma and J. Liu, Nanoparticulate WN/Ni3C Coupling in Ceramic Coatings for Boosted Urea Electro-Oxidation, *Adv. Energy Mater.*, 2023, **13**, 2302452.

25 M. Jiang, M. Zhu, H. Wang, X. Song, J. Liang, D. Lin, C. Li, J. Cui, F. Li, X. L. Zhang, Z. Tie and Z. Jin, Rapid and Green

1708 | *Inorg. Chem. Front.*, 2024, **11**, 1703–1709

This journal is © the Partner Organisations 2024

Electric-Explosion Preparation of Spherical Indium Nanocrystals with Abundant Metal Defects for Highly-Selective CO_2 Electroreduction, *Nano Lett.*, 2023, **23**, 291–297.

26 F. Shao, J. K. Wong, Q. H. Low, M. Iannuzzi, J. Li and J. Lan, In situ spectroelectrochemical probing of CO redox landscape on copper single-crystal surfaces, *Proc. Natl. Acad. Sci. U. S. A.*, 2022, **119**, e2118166119.

27 X. Chen, X.-T. Wang, J.-B. Le, S.-M. Li, X. Wang, Y.-J. Zhang, P. Radjenovic, Y. Zhao, Y.-H. Wang, X.-M. Lin, J.-C. Dong and J.-F. Li, Revealing the role of interfacial water and key

intermediates at ruthenium surfaces in the alkaline hydrogen evolution reaction, *Nat. Commun.*, 2023, **14**, 5289.

28 D. Strmcnik, M. Uchimura, C. Wang, R. Subbaraman, N. Danilovic, D. van der Vliet, A. P. Paulikas, V. R. Stamenkovic and N. M. Markovic, Improving the hydrogen oxidation reaction rate by promotion of hydroxyl adsorption, *Nat. Chem.*, 2013, **5**, 300–306.

29 W. Deng, P. Zhang, B. Seger and J. Gong, Unraveling the rate-limiting step of two-electron transfer electrochemical reduction of carbon dioxide, *Nat. Commun.*, 2022, **13**, 803.